

# Two-Phase Learning for Overcoming Noisy Labels

Hwanjun Song, Minseok Kim, Dongmin Park, Jae-Gil Lee

KAIST

{songhwanjun, minseokkim, dongminpark, jaegil}@kaist.ac.kr

## Abstract

To counter the challenge associated with noise labels, the learning strategy of deep neural networks must be differentiated over the learning period during the training process. Therefore, we propose a novel two-phase learning method, MORPH, which automatically transitions its learning phase at the point when the network begins to rapidly memorize false-labeled samples. In the first phase, MORPH starts to update the network for all the training samples before the transition point. Without any supervision, the learning phase is converted to the next phase on the basis of the estimated best transition point. Subsequently, MORPH resumes the training of the network only for a maximal safe set, which maintains the collection of almost certainly true-labeled samples at each epoch. Owing to its two-phase learning, MORPH realizes noise-free training for any type of label noise for practical use. Moreover, extensive experiments using six datasets verify that MORPH significantly outperforms five state-of-the-art methods in terms of test error and training time.

## Introduction

Deep neural networks (DNNs) have exhibited very impressive performance in numerous machine learning tasks (Krizhevsky, Sutskever, and Hinton 2012). However, their success is conditioned on the availability of massive data with carefully annotated human labels, which are expensive and time-consuming to obtain in practice. Some in-expert sources, such as Amazon’s Mechanical Turk and surrounding tags of collected data, have been widely used to mitigate the high labeling cost, but they often yield samples with *noisy labels*. In the presence of noisy labels, DNNs easily overfit to the entire training data with any ratio of noisy labels, eventually resulting in poor generalization performance (Zhang et al. 2017; Song et al. 2020b).

A popular approach to deal with noisy labels is “sample selection,” which involves selecting true-labeled samples from noisy training data (Jiang et al. 2018; Han et al. 2018; Shen and Sanghavi 2019; Chen et al. 2019). Here,  $(1 - \tau) \times 100\%$  of the *small-loss* training samples are typically treated as true-labeled samples and subsequently used to robustly update a DNN, where  $\tau \in [0, 1]$  is the noise rate. Notably, the aforementioned *small-loss trick* is satisfactorily justified by the *memorization effect* (Arpit et al.

2017) that DNNs tend to learn clean samples first and then gradually memorize all the noisy samples. In practice, Han et al. (2018) empirically proved that training on such small-loss samples yields considerably better generalization performance for artificial noise scenarios.

Despite its great success, a recent study (Song, Kim, and Lee 2019) has argued that the performance of the small-loss trick becomes considerably worse depending on the type of label noise. For instance, the small-loss trick satisfactorily separates the true-labeled samples from the false-labeled ones in *symmetric noise* (Figure 1(a)), but many false-labeled samples are misclassified as true-labeled ones because both the distributions overlap closely in *asymmetric* and *real-world noises* (Figures 1(b) and 1(c)), both of which are more *realistic* than symmetric noise (Ren et al. 2018; Yu et al. 2019; Song, Kim, and Lee 2019). Nevertheless, supporting *any* type of label noise has been underexplored yet, though it is a main challenge for sample selection.

In this regard, we have thoroughly investigated the memorization of a DNN on *real-world* noisy training samples and, consequently, observed the existence of *two* learning periods in Figure 2(a): (i) the “*noise-robust*” period where the memorization of false-labeled samples is insignificant because the network prefers memorizing easy samples at an early stage and (ii) the “*noise-prone*” period where the memorization of false-labeled samples rapidly increases because the network eventually begins memorizing all the noisy samples at a late stage of training.

Based on these findings, we propose a novel *self-transitional learning* approach called **MORPH**, which automatically transitions its learning phase when a DNN enters the “*noise-prone*” period after the “*noise-robust*” period (i.e., the dashed line in Figure 2(b)). Thus, corresponding to these two periods, our key idea is to divide the training process into two learning phases, namely *seeding* and *evolution*:

1. **Seeding:** Owing to the negligible memorization of false-labeled samples, the network update is initiated using *all* the training samples in the noise-robust period. Because the samples memorized at this time are mostly true-labeled, they are exploited as a seed to derive a *maximal safe set* in the next phase. Note that the phase transition is fully automatic without *any* supervision.
2. **Evolution:** Without memorizing false-labeled samples,

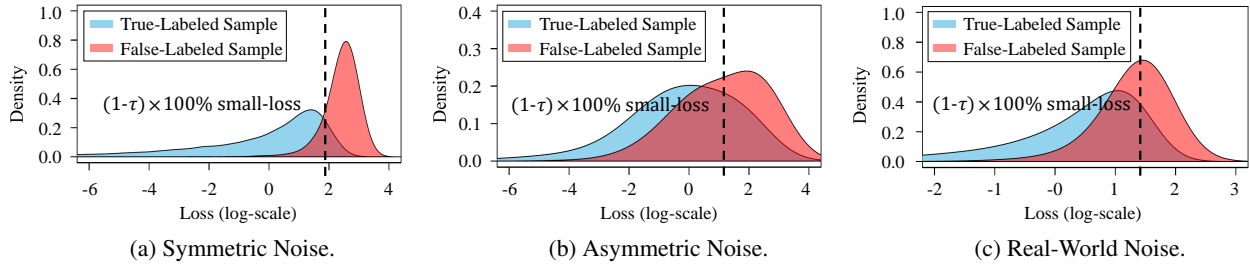


Figure 1: Loss distributions at a training accuracy of 50%: (a) and (b) show those on CIFAR-100 with two types of synthetic noises of 40%, where “symmetric noise” flips a true label into other labels with equal probability, and “asymmetric noise” flips a true label into a specific false label; (c) shows those on FOOD-101N<sup>†</sup> (Lee et al. 2018) with the real-world noise of 18.4%, where  $\dagger$  indicates the subset in which correct labels are identified.

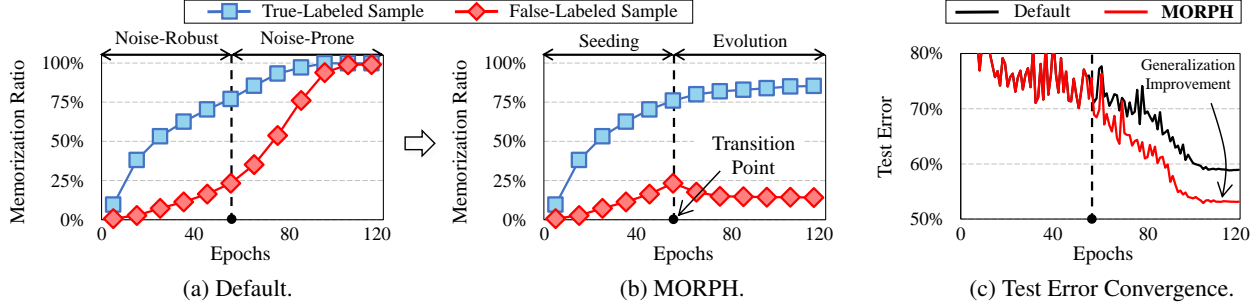


Figure 2: Key idea of MORPH: (a) and (b) show the memorization ratio when training a WideResNet-16-8 on FOOD-101N<sup>†</sup> with the real-world noise of 18.4%<sup>1</sup>, where the memorization ratio is the number of memorized (see Definition 1) true- or false-labeled samples to the total number of true- or false-labeled training samples at each epoch. “Default” is a standard training method, and “MORPH” is our proposed one; (c) contrasts the convergence of their test error.

the network evolves by being updated *only* for the maximal safe set in the noise-prone period. Then, the updated network recognizes more true-labeled samples previously indistinguishable and filters out false-labeled samples incorrectly included. This alternating process repeats per iteration so that the maximal safe set is expanded and refined in the remaining noise-prone period.

Notably, *MORPH* effectively prevents the memorization of the false-labeled samples in the noise-prone period, as shown in Figure 2(b). As a result, as shown in Figure 2(c), the generalization performance of a DNN improves remarkably even in *real-world* noise. Our main contributions are summarized as follows:

- **No Supervision for Transition:** *MORPH* performs *self-transitional* learning without *any* supervision such as a true noise rate and a clean validation set, which are usually hard to acquire in practice.
- **Noise-Type Robustness:** Only *MORPH* consistently attains high generalization performance in various noise types. Compared with state-of-the-art methods, *MORPH* significantly improved the test (or validation) error by up to 27.0pp<sup>2</sup> for the three datasets with two synthetic noises and by up to 8.90pp and 3.85pp for WebVision 1.0 and FOOD-101N with real-world noise.
- **Learning Efficiency:** Differently from other methods,

*MORPH* does not require *any* additional network or training round. Thus, it was significantly faster than other methods by up to 3.08 times.

## Related Work

Numerous studies have been conducted to address the challenge of learning from noisy labels. A typical method is using “loss correction,” which estimates the label transition matrix and corrects the loss of the samples in a mini-batch. *Bootstrap* (Reed et al. 2015) updates the network based on their own reconstruction-based objective with the notion of perceptual consistency. *F-correction* (Patrini et al. 2017) reweights the forward or backward loss of the training samples based on the label transition matrix estimated using a pre-trained normal network. *D2L* (Ma et al. 2018) employs a simple measure called local intrinsic dimensionality and then uses it to modify the forward loss in order to reduce the effects of false-labeled samples in learning. Ren et al. (2018) included a small amount of clean validation data into the training data and re-weighted the backward loss of the mini-batch samples such that the updated gradient minimized the loss of those validation data. However, this family of methods accumulates severe noise from the *false correction*, especially when the number of classes or the number of false-labeled samples is large (Han et al. 2018).

To be free from the false correction, many recent researches have adopted the method of “sample selection,” which trains the network on selected samples. This method attempts to select the true-labeled samples from the noisy

<sup>1</sup>The learning rate was decayed with cosine annealing.

<sup>2</sup>A *pp* is the abbreviation of a percentage point.

training data for updating the network. *Decouple* (Malach and Shalev-Shwartz 2017) maintains two networks simultaneously and updates the models by only using the samples with different label predictions from these two networks. Wang et al. (2018) proposed an iterative learning framework that learns deep discriminative features from well-classified noisy samples based on the local outlier factor algorithm (Breunig et al. 2000). *MentorNet* (Jiang et al. 2018) introduces a collaborative learning paradigm in which a pre-trained mentor network guides the training of a student network. Based on the small-loss criteria, the mentor provides the student with the samples whose labels are probably correct. *Co-teaching* (Han et al. 2018) and *Co-teaching+* (Yu et al. 2019) also maintain two networks, but each network selects a certain number of small-loss samples and feeds them to its peer network for further training. Compared with *Co-teaching*, *Co-teaching+* further employs the disagreement strategy of *Decouple*. *INCV* (Chen et al. 2019) randomly divides the noisy training data and then employs cross-validation to classify true-labeled samples while removing large-loss samples at each training round. *ITLM* (Shen and Sanghavi 2019) iteratively minimizes the trimmed loss by alternating between selecting a fraction of small-loss samples at the current moment and retraining the network using them. *SELFIE* (Song, Kim, and Lee 2019) trains a network on selectively refurbished samples together with small-loss samples. However, their general philosophy of simply selecting *small-loss* samples performs satisfactorily only in some cases such as symmetric noise.

Furthermore, we include recent studies combined with unsupervised and semi-supervised learning. *DM-DYR-SH* (Arazo et al. 2019) corrects the loss of training samples by modeling label noise in an unsupervised manner. *DivideMix* (Li, Socher, and Hoi 2020) treats only small-loss samples as labeled ones to adopt a semi-supervised learning technique called *MixMatch* (Berthelot et al. 2019).

Differently from these existing studies, *MORPH* is the first method that explores the noise-type robustness for sample selection. We elaborate on the technique of self-transitional learning to construct a collection of certainly true-labeled samples in a wide range of noise types.

## Preliminaries

A  $k$ -class classification problem requires training data  $\mathcal{D} = \{(x_i, y_i^*)\}_{i=1}^N$ , where  $x_i$  is a sample and  $y_i^* \in \{1, 2, \dots, k\}$  is its *true* label. Following the label noise scenario, let's consider the noisy training data  $\tilde{\mathcal{D}} = \{(x_i, \tilde{y}_i)\}_{i=1}^N$ , where  $\tilde{y}_i \in \{1, 2, \dots, k\}$  is a *noisy* label which may not be true. Moreover, in conventional training, a mini-batch  $\mathcal{B}_t = \{(x_i, \tilde{y}_i)\}_{i=1}^b$  comprises  $b$  samples drawn randomly from the noisy training data  $\tilde{\mathcal{D}}$  at time  $t$ . Given a neural network  $f(\cdot; \theta)$  parameterized by  $\theta$ , the network parameter  $\theta$  is updated along the decent direction of the expected loss on the mini-batch,

$$\theta_{t+1} = \theta_t - \alpha \nabla \left( \frac{1}{|\mathcal{B}_t|} \sum_{(x, \tilde{y}) \in \mathcal{B}_t} \mathcal{L}(f(x; \theta_t), \tilde{y}) \right), \quad (1)$$

where  $\alpha$  is the learning rate and  $\mathcal{L}$  is a specific loss function.

As for the notion of network memorization, a sample  $x$  is defined to be *memorized* by a network if the majority of its recent predictions at time  $t$  coincide with the given label, as in Definition 1.

**Definition 1. (Memorized Sample)** Let  $\hat{y}_t = f(x; \theta_t)$  be the predicted label of a sample  $x$  at time  $t$  and  $\mathcal{H}_x^t(q) = \{\hat{y}_{t_1}, \hat{y}_{t_2}, \dots, \hat{y}_{t_q}\}$  be the history of the sample  $x$  that stores the predicted labels of the recent  $q$  epochs. Next, based on  $\mathcal{H}_x^t(q)$ , the probability of a label  $y \in \{1, 2, \dots, k\}$  estimated as the label of the sample  $x$  is formulated by

$$p(y|x, t) = \frac{1}{|\mathcal{H}_x^t(q)|} \sum_{\hat{y} \in \mathcal{H}_x^t(q)} [\hat{y} = y], \quad (2)$$

where  $[S] = \begin{cases} 1, & \text{if } S \text{ is true.} \\ 0, & \text{otherwise.} \end{cases}$

Subsequently, the sample  $x$  with its noisy label  $\tilde{y}$  is *memorized* by the network with the parameter  $\theta_t$  at time  $t$  if  $\text{argmax}_y p(y|x, t) = \tilde{y}$  holds.  $\square$

## Self-Transitional Learning by *MORPH*

In this section, we propose *MORPH* which comprises the following two phases.

### Phase I: Seeding during the Noise-robust Period

Phase I initiates to update the network using *all* the training samples in a conventional way of Eq. (1) during the noise-robust period, where the memorization of false-labeled samples are suppressed. Concurrently, because most of the samples memorized until the transition point are true-labeled, *MORPH* collects them to form a *seed*, which is used as an initial maximal safe set in Phase II. The major technical challenge here is to estimate the best transition point.

The network predominantly learns true-labeled samples until the noise-prone period begins. That is, at the best phase transition point, the network (i) not only accumulates *little* noise from the false-labeled samples, (ii) but also acquires *sufficient* information from the true-labeled ones. In that sense, we introduce two memorization metrics, namely, *memorization precision (MP)* and *memorization recall (MR)* in Definition 2, which are indicators of evaluating the two aforementioned properties, respectively.

**Definition 2. (Memorization Metrics)** Let  $\mathcal{M}_t \subseteq \tilde{\mathcal{D}}$  be a set of memorized samples at time  $t$  according to Definition 1. Then, *memorization precision* and *recall* at time  $t$  are formulated by

$$MP(t) = \frac{|\{(x, \tilde{y}) \in \mathcal{M}_t : \tilde{y} = y^*\}|}{|\mathcal{M}_t|} \quad (3)$$

$$MR(t) = \frac{|\{(x, \tilde{y}) \in \mathcal{M}_t : \tilde{y} = y^*\}|}{|\{(x, \tilde{y}) \in \tilde{\mathcal{D}} : \tilde{y} = y^*\}|},$$

where  $\mathcal{M}_t = \{(x, \tilde{y}) \in \tilde{\mathcal{D}} : \text{argmax}_y p(y|x, t) = \tilde{y}\}$ .  $\square$

Figure 3 shows the change in MP and MR on the two *realistic* label noises over the training period. Owing to the memorization effect of a DNN, the two metrics were observed to naturally follow the *monotonicity* after a few warm-up epochs:

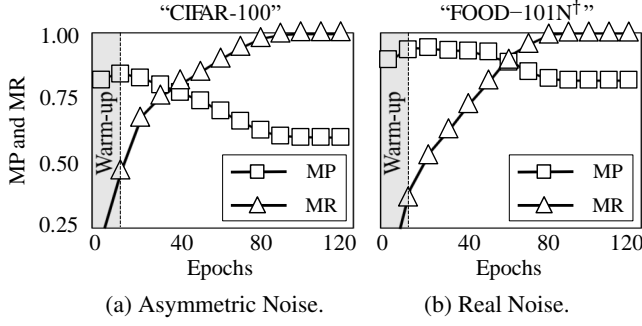


Figure 3: MP and MR when training WideResNet-16-8 on CIFAR-100 with the asymmetric noise of 40% and FOOD-101N<sup>†</sup> with the real-world noise of 18.4%.

- MP monotonically decreases because a DNN tends to memorizes true-labeled samples first and then gradually memorizes all the false-labeled samples.
- MR monotonically increases because a DNN eventually memorizes all the true-labeled samples as the training progresses.

Under the monotonicity, the best transition point is the *only cross-point* of the two metrics, i.e.,  $MP(t) = MR(t)$ , because it is the best trade-off between them. This approach is also supported by theoretical or empirical understanding of memorization in deep learning that a better generalization of a DNN is achieved when pure memorization (i.e., high MP) and its enough amount (i.e., high MR) are satisfied simultaneously (Arpit et al. 2017; Krueger et al. 2017; Zhang et al. 2020a; Li, Soltanolkotabi, and Oymak 2020; Song et al. 2020a). Then, by finding the answer of  $MP(t) = MR(t)$  in Eq. (3), the cross-point satisfies

$$|\mathcal{M}_t| = |\{(x, \tilde{y}) \in \tilde{\mathcal{D}} : \tilde{y} = y^*\}| = (1 - \tau)|\tilde{\mathcal{D}}| \quad (4)$$

$$\therefore |\mathcal{M}_t| = (1 - \tau)|\tilde{\mathcal{D}}|,$$

where  $\tau$  is the true noise rate. Because  $\tau$  is typically unknown, it is *automatically* estimated by *MORPH* to check the condition in Eq. (4) for the phase transition.

Regarding the noise rate estimation, *MORPH* fits a two-component Gaussian Mixture Model (GMM) to model the loss distribution of true-labeled and false-labeled samples because the distribution is bi-modal (Arazo et al. 2019; Pleiss et al. 2020). At each epoch, *MORPH* accumulates the loss of all the training samples and fits the GMM to the accumulated loss by using the Expectation-Maximization (EM) algorithm. The probability of a sample  $x$  being false-labeled is obtained through its posterior probability. Accordingly, the noise rate  $\tau$  is estimated by

$$\hat{\tau} = \mathbb{E}_{(x, \tilde{y}) \in \tilde{\mathcal{D}}} [p(g | \mathcal{L}(f(x; \theta_t), \tilde{y})], \quad (5)$$

where  $g$  is the Gaussian component with a larger mean (i.e., larger loss). A thorough analysis of estimating the noise rate is provided in Appendix A.

Overall, *MORPH* transitions the learning phase at time  $t_{tr}$  when the number of memorized samples is greater than or equal to the estimated number of true-labeled ones (i.e.,  $|\mathcal{M}_{t_{tr}}| \geq (1 - \hat{\tau})|\tilde{\mathcal{D}}|$ ). Please note that *MORPH* requires *neither* a true noise rate *nor* a clean validation set.

## Phase II: Evolution during the Noise-prone Period

Phase II robustly updates the network *only* using the selected clean samples called the *maximal safe set* in Definition 3. By the definition of the transition point, the initial maximal safe set obtained in Phase I is qualitatively clean and quantitatively sufficient (i.e., high MP and MR); however, it can be further improved by (i) including more true-labeled samples previously indistinguishable and (ii) filtering out false-labeled samples incorrectly included. Hence, the set is expanded and refined by iteratively updating the network with the current set  $\mathcal{S}_t$  as in Eq. (6) and deriving a more refined set  $\mathcal{S}_{t+1}$  as in Eq. (7). By the fact that false-labeled samples are easily forgotten (Toneva et al. 2019), the network keeps more true-labeled samples  $\mathcal{C}$  owing to the robust update, while forgetting the false-labeled samples  $\mathcal{R}$  which were incorrectly memorized earlier. In this way, *MORPH* becomes better generalized to almost all true-labeled samples through the evolution of the maximal safe set.

**Definition 3. (Maximal Safe Set)** A *maximal safe set*  $\mathcal{S}_t$  is defined as the set of samples expected to be true-labeled at time  $t (\geq t_{tr})$ , where  $t_{tr}$  is the transition point. It starts from  $\mathcal{S}_{t_{tr}} = \mathcal{M}_{t_{tr}}$ , and is managed as follows:

1. The refinement of the maximal safe set  $\mathcal{S}_t$  accompanies the update of the network parameter  $\theta_t$ . To be free from memorizing false-labeled samples in Phase II, the network parameter  $\theta_{t+1}$  is robustly learned only using the samples in  $\mathcal{S}_t$  out of the mini-batch  $\mathcal{B}_t$  by

$$\theta_{t+1} = \theta_t - \alpha \nabla \left( \frac{1}{|\mathcal{B}_t \cap \mathcal{S}_t|} \sum_{(x, \tilde{y}) \in (\mathcal{B}_t \cap \mathcal{S}_t)} \mathcal{L}(f(x; \theta_t), \tilde{y}) \right). \quad (6)$$

2. Then,  $\mathcal{S}_{t+1}$  reflects the changes by the network update at time  $t + 1$ , i.e., newly memorized samples  $\mathcal{C}_t$  and newly forgotten samples  $\mathcal{R}_t$ , as formulated by

$$\mathcal{S}_{t+1} = \mathcal{S}_t + \mathcal{C} - \mathcal{R}, \quad \text{where} \quad (7)$$

$$\mathcal{C} = \{(x, \tilde{y}) \in (\mathcal{B}_t \cap \mathcal{S}_t^c) : \text{argmax}_y p(y|x, t+1) = \tilde{y}\},$$

$$\mathcal{R} = \{(x, \tilde{y}) \in (\mathcal{B}_t \cap \mathcal{S}_t) : \text{argmax}_y p(y|x, t+1) \neq \tilde{y}\}. \quad \square$$

To reduce the possibility of the overfitting to a small *initial* set, which is typically observed with a very high noise rate, *MORPH* combines the supervised loss in Eq. (6) with an unsupervised loss  $\mathcal{J}(\theta_t)$  widely known as *consistency regularization* (Laine and Aila 2017; Zhang et al. 2020b). Without relying on possibly unreliable labels, this regularization effectively helps learn the *dark knowledge* (Hinton, Vinyals, and Dean 2015) from *all* the training samples by penalizing the prediction difference between the original sample  $x$  and its augmented sample  $\hat{x}$ . (For the experiments,  $\hat{x}$ 's were generated by random crops and horizontal flips.) Hence, the update rule is finally defined by

$$\theta_{t+1} = \theta_t - \alpha \nabla \left( \frac{1}{|\mathcal{B}_t \cap \mathcal{S}_t|} \sum_{x \in (\mathcal{B}_t \cap \mathcal{S}_t)} \mathcal{L}(f(x; \theta_t), \tilde{y}) + w(t) \mathcal{J}(\theta_t) \right),$$

$$\text{where } \mathcal{J}(\theta_t) = \frac{1}{\mathcal{B}_t} \sum_{x \in \mathcal{B}_t} \|z(x; \theta_t) - z(\hat{x}; \theta_t)\|_2^2, \quad (8)$$

---

**Algorithm 1** MORPH

---

INPUT:  $\tilde{\mathcal{D}}$ : data,  $epochs$ : total number of epochs,  $q$ : history length,  $w_{max}$ : maximum weight for  $\mathcal{J}$   
 OUTPUT:  $\theta_t$ : network parameters,  $\mathcal{S}_t$ : final safe set

- 1:  $t \leftarrow 1$ ;  $\mathcal{S}_t \leftarrow \emptyset$ ;
- 2:  $\theta_t \leftarrow$  Initialize the network parameter;
- 3: /\* **I. Seeding during Noise-Robust Period \*/**
- 4: **for**  $i = 1$  to  $epochs$  **do**
- 5:   **for**  $j = 1$  to  $|\tilde{\mathcal{D}}|/|\mathcal{B}_t|$  **do**
- 6:     Draw a mini-batch  $\mathcal{B}_t$  from  $\tilde{\mathcal{D}}$ ;
- 7:     /\* Standard update by Eq. (1) \*/
- 8:      $\theta_{t+1} = \theta_t - \alpha \nabla \left( \frac{1}{|\mathcal{B}_t|} \sum_{x \in \mathcal{B}_t} \mathcal{L}(f(x; \theta_t), \tilde{y}) \right)$ ;
- 9:      $t \leftarrow t + 1$ ;
- 10:    /\* Noise rate estimation by Eq. (5) \*/
- 11:     $\hat{\tau} \leftarrow \mathbb{E}_{(x, \tilde{y}) \in \tilde{\mathcal{D}}} [p(g | \mathcal{L}(f(x; \theta_t), \tilde{y}))]$ ;
- 12:    /\* Checking the phase transition condition \*/
- 13:    **if**  $|\mathcal{M}_t| \geq (1 - \hat{\tau})|\tilde{\mathcal{D}}|$  **then**
- 14:     /\* Assigning the initial maximal safe set \*/
- 15:      $t_{tr} \leftarrow t$ ;  $\mathcal{S}_{t_{tr}} \leftarrow \mathcal{M}_{t_{tr}}$ ;
- 16: /\* **II. Evolution during Noise-Prone Period \*/**
- 17: **for**  $i = t_{tr}|\mathcal{B}_t|/|\tilde{\mathcal{D}}| + 1$  to  $epochs$  **do**
- 18:   **for**  $j = 1$  to  $|\tilde{\mathcal{D}}|/|\mathcal{B}_t|$  **do**
- 19:     Draw a mini-batch  $\mathcal{B}_t$  from  $\tilde{\mathcal{D}}$ ;
- 20:     /\* Robust update by Eq. (8) \*/
- 21:      $\theta_{t+1} = \theta_t - \alpha \nabla \left( \frac{1}{|\mathcal{B}_t \cap \mathcal{S}_t|} \sum_{x \in (\mathcal{B}_t \cap \mathcal{S}_t)} \mathcal{L}(f(x; \theta_t), \tilde{y}) + w(t) \mathcal{J}(\theta_t) \right)$ ;
- 22:     /\* Updating the maximal safe set by Eq. (7) \*/
- 23:      $\mathcal{S}_{t+1} \leftarrow \mathcal{S}_t + \mathcal{C} - \mathcal{R}$ ;
- 24:      $t \leftarrow t + 1$ ;
- 25: **return**  $\theta_t, \mathcal{S}_t$ ;

---

where  $z(x; \theta_t)$  is the softmax vector of a sample  $x$  and  $w(t)$  is a Gaussian ramp-up function to gradually increase the weight to the maximum value  $w_{max}$ . According to our ablation study in Appendix B.1, the robustness of *MORPH* is considerably enhanced by using the regularization.

### Algorithm Pseudocode

Algorithm 1 describes the overall procedure of *MORPH*, which is self-explanatory. The main “additional” costs of *MORPH* are (i) the estimation of the noise rate (Line 11) and (ii) the additional inference step for the consistency regularization (Line 21). Because the noise rate is estimated using the EM algorithm once per epoch, its cost is negligible compared with that of the inference steps of a complex network. Thus, the additional inference in Phase II is the only part that increases the time complexity. Nevertheless, the additional cost is relatively *cheap* considering that other sample selection methods require either an additional network or multiple training rounds. We empirically show that *MORPH* is 1.13–3.08 times faster than other methods in Appendix B.2.

## Evaluation

### Datasets and Implementation Details

We performed an image classification task on *five* benchmark datasets: CIFAR-10 (Krizhevsky, Nair, and Hinton

2014), CIFAR-100 (Krizhevsky, Nair, and Hinton 2014), Tiny-ImageNet (Krizhevsky, Sutskever, and Hinton 2012), WebVision 1.0 (Li et al. 2017), and FOOD-101N (Lee et al. 2018). As all the labels in CIFAR and Tiny-ImageNet are clean, we artificially corrupted the labels in these datasets following the previous work (Han et al. 2018; Yu et al. 2019). We applied two synthetic label noises: *i*) *symmetric noise* and *ii*) *asymmetric noise*. Random crops and horizontal flips were applied for data augmentation.

For CIFAR and Tiny-ImageNet, we trained a Wide ResNet-16-8 (Zagoruyko and Komodakis 2016) from scratch using SGD with a momentum of 0.9, a batch size of 128, a dropout of 0.1, and a weight decay of 0.0005. The network was trained for 120 epochs with an initial learning rate of 0.1, which was decayed with cosine annealing (Loshchilov and Hutter 2016). For the hyperparameters, we used the best history length  $q = 10$  and maximum weight  $w_{max} = 5.0$ , which were obtained via a grid search (see Appendix B.3 for details). The  $w$  value gradually increased from 0 to  $w_{max}$  using a Gaussian ramp-up function as the network with a large  $w$  gets stuck in a degenerate solution at the beginning (Laine and Aila 2017).

WebVision 1.0 and FOOD-101N are two large-scale datasets with real-world label noise (Lee et al. 2018; Li et al. 2017). WebVision 1.0 contains 2.4M images crawled from websites using the 1,000 concepts in ImageNet ILSVRC12 (Deng et al. 2009), and FOOD-101N contains 310K food images crawled from websites with the FOOD-101 taxonomy (Bossard, Guillaumin, and Van Gool 2014). We followed the same experimental configuration in the previous work. For WebVision 1.0, we trained an Inception ResNet-V2 (Szegedy et al. 2017) from scratch for the first 50 classes of the Google image subset (Chen et al. 2019); for FOOD-101N, we fine-tuned a ResNet-50 with the ImageNet pretrained weights for the entire training set (Lee et al. 2018). Please see Appendix C.1 and Appendix C.2 for the details of benchmark datasets and training configurations.

All the algorithms were implemented using TensorFlow 2.1.0 and executed using 16 NVIDIA Titan Volta GPUs. In support of reliable evaluation, we repeated every task *thrice* and reported the average test (or validation) error as well as the average training time.

### Robustness Comparison with Synthetic Noises

We compared *MORPH* with the *five* state-of-the-art sample selection methods: *Co-teaching* (Han et al. 2018), *Co-teaching+* (Yu et al. 2019), *INCV* (Chen et al. 2019), *ITLM* (Shen and Sanghavi 2019), and *SELFIE* (Song, Kim, and Lee 2019). The other methods were re-implemented by the authors for fair comparison, and their hyperparameters were configured to the best values, as detailed in Appendix C.3. In addition, the comparison with *DM-DYR-SH* (Arazo et al. 2019) and *DivideMix* (Li, Socher, and Hoi 2020), which are in fact not directly comparable with *MORPH*, is discussed in Appendix C.4.

Figures 4 and 5 show the test errors of the six sample selection methods with varying *asymmetric* and *symmetric* noise rates. See Appendix D.1 for the tabular reports.

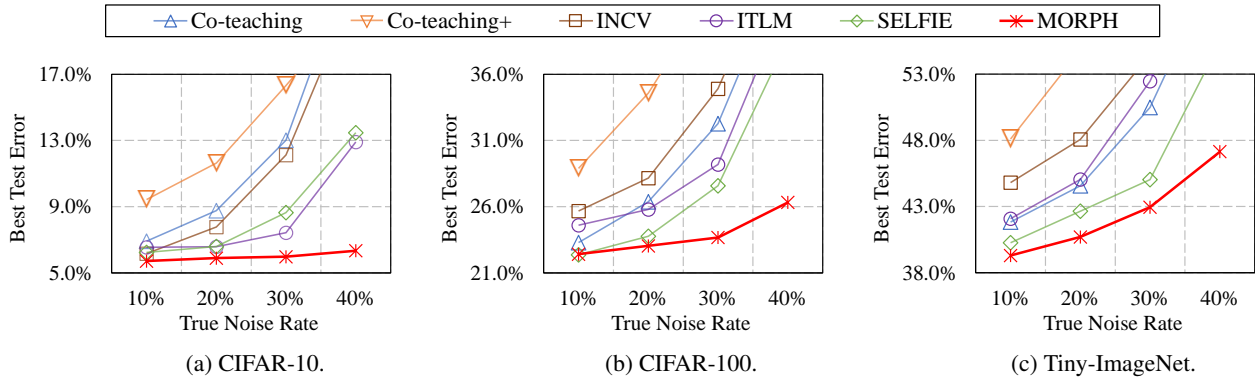


Figure 4: Best test errors on three datasets using WideResNet with varying asymmetric noise rates.

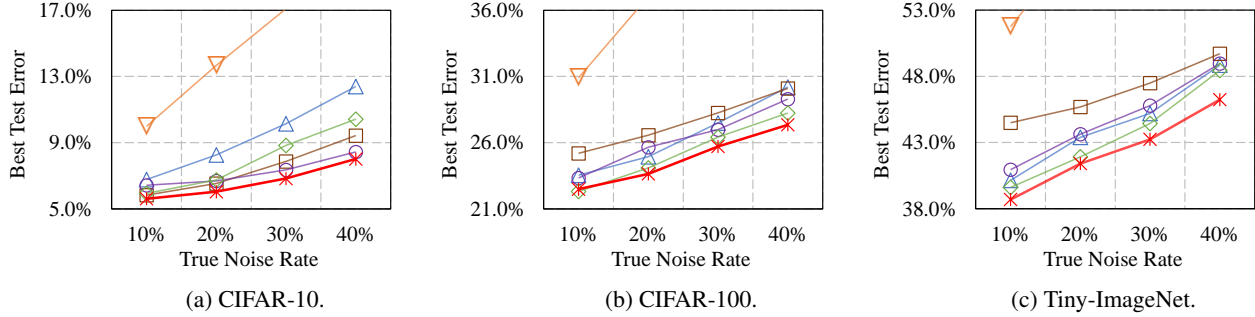


Figure 5: Best test errors on three datasets using WideResNet with varying symmetric noise rates.

Method	WebVision Val.	ILSVRC12 Val.
<i>F</i> -correction (Patrini et al. 2017)	38.88 (17.32)	42.64 (17.64)
<i>Decouple</i> (Malach et al. 2017)	37.46 (15.26)	41.74 (17.74)
<i>Co-teaching</i> (Han et al. 2018)	36.42 (14.80)	38.52 (15.30)
<i>MentorNet</i> (Jiang et al. 2018)	37.00 (18.60)	42.20 (20.08)
<i>D2L</i> (Ma et al. 2018)	37.32 (16.00)	42.20 (18.64)
<i>INCV</i> (Chen et al. 2019)	34.76 (14.66)	38.40 (15.02)
<b><i>MORPH</i></b>	<b>29.98 (11.33)</b>	<b>33.09 (12.62)</b>

Table 1: Comparison with state-of-the-art methods trained on WebVision V1. The value outside (inside) the parentheses denotes the top-1 (top-5) classification error (%) on the WebVision validation set and the ImageNet ILSVRC12 validation set. The results for baseline methods are borrowed from (Chen et al. 2019).

**Asymmetric Noise** *MORPH* generally achieved the lowest test errors with respect to a wide range of noise rates. The error reduction became larger as the noise rate increased, reaching 6.6pp–27.0pp at a heavy noise rate of 40%. In contrast, the performance of the other methods worsened rapidly, because of the limitation of their small-loss trick, which could not distinguish well true-labeled samples from false-labeled samples in asymmetric and real-world noises, as illustrated in Figures 1(b) and (c).

**Symmetric Noise** *MORPH* generally outperformed the other methods again, though the error reduction was relatively small, i.e., 0.42pp–26.3pp at a heavy noise rate of 40%. The small-loss trick was turned out to be appropriate for symmetric noise, as illustrated in Figure 1(a).

Method	FOOD-101 Val.
<i>Cross-Entropy</i> (Lee et al. 2018)	18.56
<i>Weakly Supervised</i> (Zhuang et al. 2017)	16.57
<i>CleanNet</i> ( $w_{hard}$ ) <sup>†</sup> (Lee et al. 2018)	16.53
<i>CleanNet</i> ( $w_{soft}$ ) <sup>†</sup> (Lee et al. 2018)	16.05
<i>Guidance Learning</i> <sup>†</sup> (Li et al. 2020)	15.80
<b><i>MORPH</i></b>	<b>14.71</b>

Table 2: Comparison with state-of-the-art methods trained on FOOD-101N. The value denotes the top-1 classification error (%) on the FOOD-101 validation set. The results for baseline methods are borrowed from (Lee et al. 2018; Li et al. 2020). <sup>†</sup> indicates that extra clean (or verification) labels were used for supervision.

Putting them together, we contend that only *MORPH* realizes *noise type robustness*, evidenced by consistently low test errors in both asymmetric and symmetric noises.

## Robustness Comparison with Real-World Noises

Tables 1 and 2 summarize the results on WebVision V1 and FOOD-101N, respectively. *MORPH* maintained its dominance over multiple state-of-the-art methods for *real-world* label noise as well. It improved the top-1 validation error by 4.44pp–8.90pp and 1.09pp–3.85pp in WebVision V1 and FOOD-101N, respectively. This lowest error of *MORPH* in FOOD-101N was achieved even without extra supervision from the clean (or verification) labels.

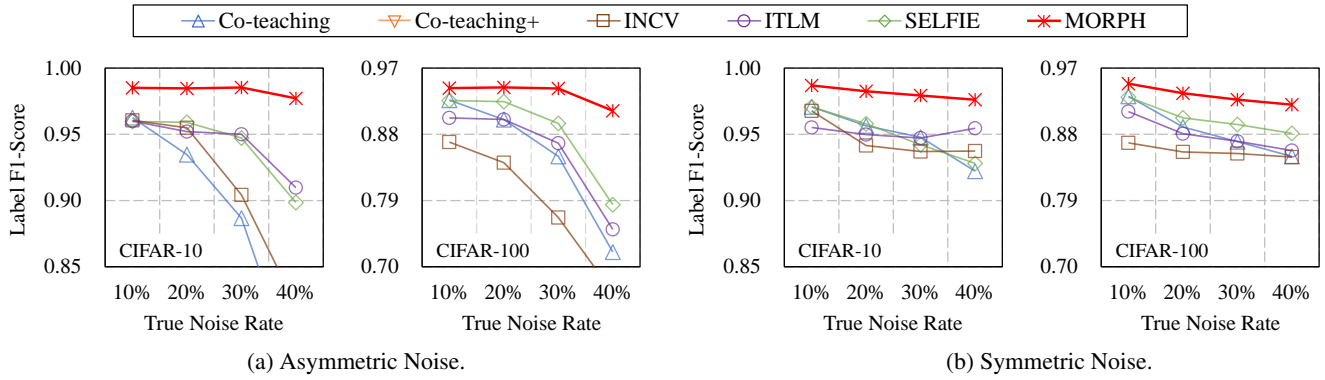


Figure 6: Label F1-Scores on two CIFARs data using WideResNet with varying noise rates.

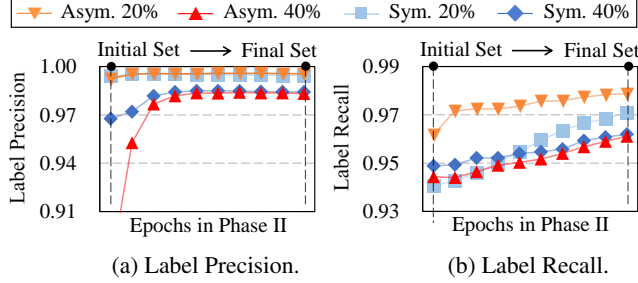


Figure 7: Evolution of the maximal safe set in Phase II using WideResNet on CIFAR-10 with two synthetic noises.

### Analysis on Selected Clean Samples

The superior robustness of *MORPH* is attributed to its high *label precision* (LP) and *label recall* (LR), which are calculated by replacing  $\mathcal{M}$  for MP and MR in Eq. (3) with the set of selected clean samples (Han et al. 2018). Hence, we compare *MORPH* with the other five sample selection methods in terms of the *label F1-score*,

$$\text{Label F1-Score} = (2 \cdot LP \cdot LR) / (LP + LR). \quad (9)$$

To evaluate the label F1-score, *MORPH* used its final maximal safe set, *Co-teaching*(+) and *SELFIE* used the samples selected during their last epoch, and *INCV* and *ITLM* used the samples selected for their final training round. Figure 6 shows their label F1-scores. Only *MORPH* achieved consistently high label F1-scores of over 0.91 in all the cases. This result corroborates that *MORPH* identifies true-labeled samples with high precision and recall regardless of the noise type and rate.

### Evolution of the Maximal Safe Set

Figure 7 shows the LP and LR values on the maximal safe set obtained at each epoch since Phase II begins. At the beginning of Phase II, both LP and LR already exhibited fairly high values because the initial set is derived from the samples memorized at the transition point, which is best compromise between MP and MR. Moreover, they increased gradually as the training in Phase II progressed by filtering out false-labeled samples incorrectly included and adding more true-labeled ones previously indistinguishable. Notably, their improvement was consistently observed regardless of the noise type and rate, thereby achieving remarkably

Transition Point	Early	Best	Late		
A value $\alpha$	+10%	+5%	+0%	-5%	-10%
CIFAR-10 (Sym.)	8.71	8.37	<b>8.01</b>	9.39	9.75
CIFAR-10 (Asym.)	7.53	<b>6.20</b>	6.34	7.43	8.08
CIFAR-100 (Sym.)	29.8	28.5	<b>27.4</b>	28.1	28.5
CIFAR-100 (Asym.)	28.3	27.2	<b>26.3</b>	27.0	28.9

Table 3: Best test errors (%) of *MORPH* with early or late transition based on the best point, where  $\alpha$  is added to the estimated noise rate in Eq. (4) to force early or late transition. CIFARs with two synthetic noises of 40% were used.

high LP and LR at the end. The high F1-score of *MORPH* is well supported by this evolution of the safe set.

### Optimality of the Best Transition Point

To verify the optimality of the best transition point, we investigated the performance change of *MORPH* when forcing early or late transition. Table 3 shows the test errors of *MORPH* with early or late transition based on the estimated best transition point. The best test error was generally achieved at the estimated best point other than those around the best point. The more deviated the transition point from the best point, the higher the test error. Overall, this empirical result confirms the optimality of the best transition point estimated by *MORPH*.

## Conclusion

We proposed a novel self-transitional learning scheme called *MORPH* for noisy training data. The first phase exploits all training samples and estimates the most optimal transition point. The second phase completes the rest of the training process using only a maximal safe set with high label precision and recall. *MORPH* can be easily applied to many real-world cases because it requires neither a true noise rate nor a clean validation set. Through extensive experiments using various real-world and simulated noisy datasets, we verified that *MORPH* consistently exhibited significant improvement in both robustness and efficiency compared with state-of-the-art methods. Overall, we believe that the division of the training process into two phases unveils a new approach to robust training and can inspire subsequent studies.

## References

Arazo, E.; Ortego, D.; Albert, P.; O'Connor, N.; and McGuinness, K. 2019. Unsupervised Label Noise Modeling and Loss Correction. In *ICML*, 312–321.

Arpit, D.; Jastrzebski, S.; Ballas, N.; Krueger, D.; Bengio, E.; Kanwal, M. S.; Maharaj, T.; Fischer, A.; Courville, A.; Bengio, Y.; et al. 2017. A closer look at memorization in deep networks. In *ICML*, 233–242.

Berthelot, D.; Carlini, N.; Goodfellow, I.; Papernot, N.; Oliver, A.; and Raffel, C. A. 2019. MixMatch: A holistic approach to semi-supervised learning. In *NeurIPS*, 5049–5059.

Bossard, L.; Guillaumin, M.; and Van Gool, L. 2014. Food-101-mining discriminative components with random forests. In *ECCV*, 446–461.

Breunig, M. M.; Kriegel, H.-P.; Ng, R. T.; and Sander, J. 2000. LOF: Identifying density-based local outliers. *ACM SIGMOD Record* 29(2): 93–104.

Chen, P.; Liao, B. B.; Chen, G.; and Zhang, S. 2019. Understanding and utilizing deep neural networks trained with noisy labels. In *ICML*, 1062–1070.

Deng, J.; Dong, W.; Socher, R.; Li, L.-J.; Li, K.; and Fei-Fei, L. 2009. Imagenet: A large-scale hierarchical image database. In *CVPR*, 248–255.

Han, B.; Yao, Q.; Yu, X.; Niu, G.; Xu, M.; Hu, W.; Tsang, I.; and Sugiyama, M. 2018. Co-teaching: Robust training of deep neural networks with extremely noisy labels. In *NeurIPS*, 8536–8546.

Hinton, G.; Vinyals, O.; and Dean, J. 2015. Distilling the knowledge in a neural network. *CoRR* .

Jiang, L.; Zhou, Z.; Leung, T.; Li, L.-J.; and Fei-Fei, L. 2018. MentorNet: Learning data-driven curriculum for very deep neural networks on corrupted labels. In *ICML*, 2309–2318.

Kremer, J.; Sha, F.; and Igel, C. 2018. Robust active label correction. In *AISTATS*, 308–316.

Krizhevsky, A.; Nair, V.; and Hinton, G. 2014. CIFAR-10 and CIFAR-100 datasets. <https://www.cs.toronto.edu/~kriz/cifar.html>.

Krizhevsky, A.; Sutskever, I.; and Hinton, G. E. 2012. ImageNet classification with deep convolutional neural networks. In *NeurIPS*, 1097–1105.

Krueger, D.; Ballas, N.; Jastrzebski, S.; Arpit, D.; Kanwal, M. S.; Maharaj, T.; Bengio, E.; Fischer, A.; and Courville, A. 2017. Deep nets don't learn via memorization. In *ICLRW*.

Laine, S.; and Aila, T. 2017. Temporal ensembling for semi-supervised learning. In *ICLR*.

Lee, K.-H.; He, X.; Zhang, L.; and Yang, L. 2018. CleanNet: Transfer learning for scalable image classifier training with label noise. In *CVPR*, 5447–5456.

Li, J.; Socher, R.; and Hoi, S. C. 2020. DivideMix: Learning with noisy labels as semi-supervised learning. In *ICLR*.

Li, M.; Soltanolkotabi, M.; and Oymak, S. 2020. Gradient descent with early stopping is provably robust to label noise for overparameterized neural networks. In *AISTATS*, 4313–4324.

Li, Q.; Peng, X.; Cao, L.; Du, W.; Xing, H.; Qiao, Y.; and Peng, Q. 2020. Product image recognition with guidance learning and noisy supervision. *Computer Vision and Image Understanding* 102963.

Li, W.; Wang, L.; Li, W.; Agustsson, E.; and Van Gool, L. 2017. Webvision database: Visual learning and understanding from web data. *arXiv preprint arXiv:1708.02862* .

Loshchilov, I.; and Hutter, F. 2016. SGDR: Stochastic gradient descent with warm restarts. In *ICLR*.

Ma, X.; Wang, Y.; Houle, M. E.; Zhou, S.; Erfani, S. M.; Xia, S.-T.; Wijewickrema, S.; and Bailey, J. 2018. Dimensionality-Driven learning with noisy labels. In *ICML*, 3361–3370.

Ma, Z.; and Leijon, A. 2011. Bayesian estimation of beta mixture models with variational inference. *IEEE Transactions on Pattern Analysis and Machine Intelligence* 33(11): 2160–2173.

Malach, E.; and Shalev-Shwartz, S. 2017. Decoupling “when to update” from “how to update”. In *NeurIPS*, 960–970.

Patrini, G.; Rozza, A.; Menon, A. K.; Nock, R.; and Qu, L. 2017. Making deep neural networks robust to label noise: A loss correction approach. In *CVPR*, 2233–2241.

Pleiss, G.; Zhang, T.; Elenberg, E. R.; and Weinberger, K. Q. 2020. Detecting Noisy Training Data with Loss Curves. URL <https://openreview.net/forum?id=HyenUkrtDB>.

Reed, S.; Lee, H.; Anguelov, D.; Szegedy, C.; Erhan, D.; and Rabinovich, A. 2015. Training deep neural networks on noisy labels with bootstrapping. In *ICLR*.

Ren, M.; Zeng, W.; Yang, B.; and Urtasun, R. 2018. Learning to reweight examples for robust deep learning. In *ICML*, 4334–4343.

Shen, Y.; and Sanghavi, S. 2019. Learning with bad training data via iterative trimmed loss minimization. In *ICML*, 5739–5748.

Song, H.; Kim, M.; and Lee, J.-G. 2019. SELFIE: Refurbishing unclean samples for robust deep learning. In *ICML*, 5907–5915.

Song, H.; Kim, M.; Park, D.; and Lee, J.-G. 2020a. How does early stopping help generalization against label noise? *ICMLW* .

Song, H.; Kim, M.; Park, D.; and Lee, J.-G. 2020b. Learning from noisy labels with deep neural networks: A survey. *arXiv preprint arXiv:2007.08199* .

Szegedy, C.; Ioffe, S.; Vanhoucke, V.; and Alemi, A. A. 2017. Inception-v4, inception-resnet and the impact of residual connections on learning. In *AAAI*.

Toneva, M.; Sordoni, A.; Combes, R. T. d.; Trischler, A.; Bengio, Y.; and Gordon, G. J. 2019. An empirical study of

example forgetting during deep neural network learning. In *ICLR*.

Wang, Y.; Liu, W.; Ma, X.; Bailey, J.; Zha, H.; Song, L.; and Xia, S.-T. 2018. Iterative learning with open-set noisy labels. In *CVPR*, 8688–8696.

Yu, X.; Han, B.; Yao, J.; Niu, G.; Tsang, I.; and Sugiyama, M. 2019. How does disagreement help generalization against label corruption? In *ICML*, 7164–7173.

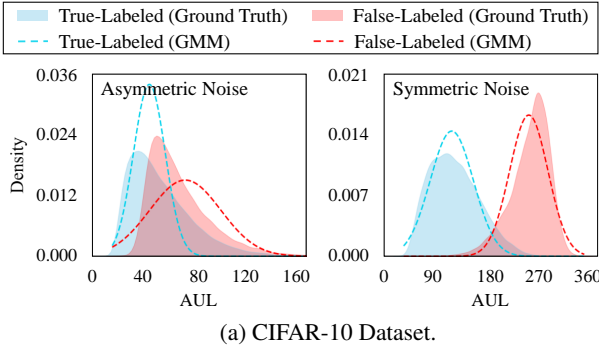
Zagoruyko, S.; and Komodakis, N. 2016. Wide residual networks. In *BMVC*.

Zhang, C.; Bengio, S.; Hardt, M.; Mozer, M. C.; and Singer, Y. 2020a. Identity Crisis: Memorization and generalization under extreme overparameterization. In *ICLR*.

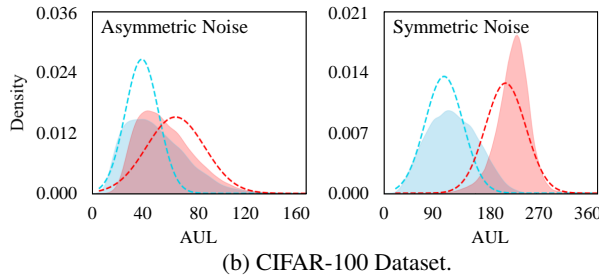
Zhang, C.; Bengio, S.; Hardt, M.; Recht, B.; and Vinyals, O. 2017. Understanding deep learning requires rethinking generalization. In *ICLR*.

Zhang, H.; Zhang, Z.; Odena, A.; and Lee, H. 2020b. Consistency regularization for generative adversarial networks. In *ICLR*.

Zhuang, B.; Liu, L.; Li, Y.; Shen, C.; and Reid, I. 2017. Attend in groups: A weakly-supervised deep learning framework for learning from web data. In *CVPR*, 1878–1887.



(a) CIFAR-10 Dataset.



(b) CIFAR-100 Dataset.

Figure 8: AUL distributions of true-labeled and false-labeled samples using the ground-truth label and the GMM on two CIFAR datasets with two synthetic noises of 40%.

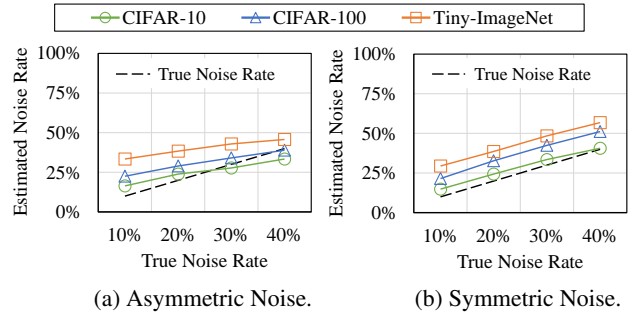
## A Noise Rate Estimation

Recently, numerous studies have provided practical algorithms for estimating the noise rate of the training data (Kremer, Sha, and Igel 2018; Arazo et al. 2019; Chen et al. 2019; Pleiss et al. 2020). Because the best transition point is found by estimating the noise rate, we explored two widely used methods in the literature, as follows:

1. **Gaussian Mixture Model (GMM):** The first method is exploiting a one-dimensional and two-component GMM to model the loss distribution of true-labeled and false-labeled samples (Arazo et al. 2019; Pleiss et al. 2020). Because the loss distribution tends to be bimodal, the probability of a sample being a false-labeled sample is obtained through its posterior probability. Subsequently, the noise rate is estimated by computing the expectation of the posterior probability for all the training samples. However, in considering that the network eventually memorizes all the training samples, the training loss becomes less separable by the GMM as the training progresses. Thus, we computed the *Area Under the Loss curve* (AUL) (Pleiss et al. 2020), which is the sum of the samples' training losses obtained from all previous training epochs. The main benefit of the AUL is that its distribution remains separable even after the loss signal decays in later epochs. Therefore, as shown in Figure 8, the loss distributions of true-labeled and false-labeled samples are modeled by fitting the GMM to the AULs of all the training samples, and the noise rate at time  $t$  is estimated by

$$\hat{\tau} = \mathbb{E}_{(x, \tilde{y}) \in \tilde{\mathcal{D}}} [p(g | AUL_t(x, \tilde{y}))],$$

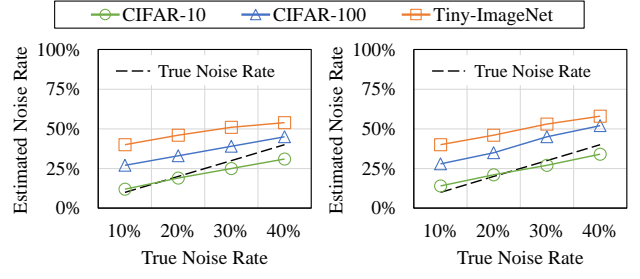
$$\text{where } AUL_t(x, \tilde{y}) = \sum_{i=1}^t \mathcal{L}(f(x; \theta_t), \tilde{y}) \quad (10)$$



(a) Asymmetric Noise.

(b) Symmetric Noise.

Figure 9: Estimation with GMM.



(a) Asymmetric Noise.

(b) Symmetric Noise.

Figure 10: Estimation with Cross-Validation.

and  $g$  is the Gaussian component with a larger mean (i.e., larger AUL).

2. **Cross-Validation:** The second method is estimating the noise rate by applying cross-validation on two randomly divided noisy training datasets  $\tilde{\mathcal{D}}_1$  and  $\tilde{\mathcal{D}}_2$  (Chen et al. 2019). Under the assumptions that these two datasets share exactly the same label transition matrix, the noise rate quantifies the test accuracy of DNNs, which are trained and tested on previously mentioned noisy datasets  $\tilde{\mathcal{D}}_1$  and  $\tilde{\mathcal{D}}_2$ , respectively. In the case of synthetic noises, the test accuracy is approximated by a quadratic function of the noise rate. Therefore, the noise rate can be estimated from the test accuracy obtained by the cross-validation. Refer to (Chen et al. 2019) for details.

Figures 9 and 10 show the estimated noise rates using the GMM and cross-validation when training a WideResNet-16-8 on three benchmark datasets with varying noise rates. Generally, both methods performed well on the easy dataset (i.e., CIFAR-10), but their performance worsened as the training difficulty increased from CIFAR-10 to Tiny-ImageNet because the true-labeled but hard samples are *not* clearly distinguishable from the false-labeled samples. Nevertheless, the GMM showed considerably better performance than the cross-validation even in the two difficult datasets, CIFAR-100 and Tiny-ImageNet. Thus, we adopted the GMM for estimating the noise rate in *MORPH*.

## B Supplementary Evaluation

### B.1 Effect of Consistency Regularization

Figure 11 shows the effect of the consistency regularization. Interestingly, as shown in Figure 11(a), the test error

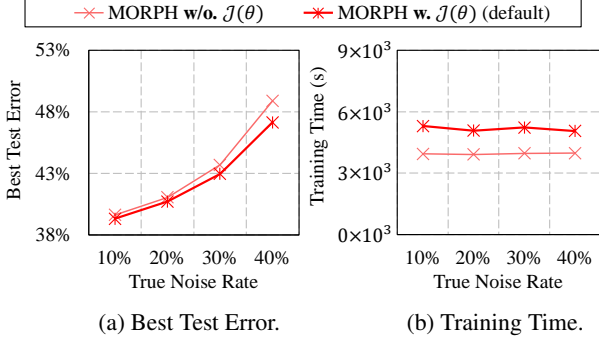


Figure 11: Effect of the consistency loss  $\mathcal{J}(\theta)$  on Tiny-ImageNet with asymmetric noise.

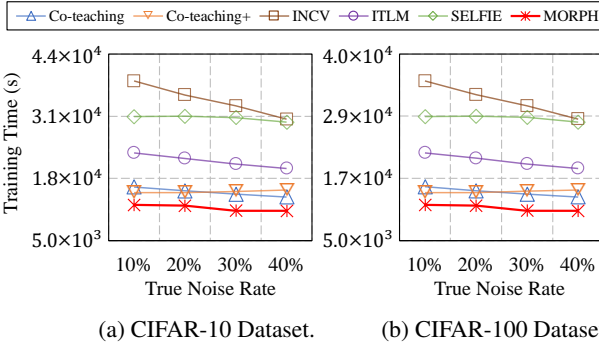


Figure 12: Training time on CIFAR-10 and CIFAR-100 datasets with asymmetric noise.

of *MORPH* was further improved by adding the consistency loss in Eq. (8). The higher the noise rate, the greater the benefit because the overfitting issue caused by a smaller size of the initial maximal safe set is mitigated. Regarding the training time, as shown in Figure 11(b), the regularization slightly slowed down the training speed owing to the extra inference steps. Because *MORPH* achieved lower test error than the other robust methods even *without* the regularization (see Appendix D.2 for details), practitioners may skip employing the regularization if their time budgets are restricted.

## B.2 Efficiency Comparison

Another advantage of *MORPH* is its efficiency in training the network. Figure 12 shows the training time of the six sample selection methods on two CIFAR datasets. *MORPH* was the fastest in each case because of its relatively cheap additional costs. Overall, *MORPH* was 1.13–3.08 times faster than the other methods. The difference between the training time of the remaining methods tended to be determined by the total number of training rounds, which is represented by one of their hyperparameters. The general trend in training time remained the same for other datasets as well. See Table 6 in Appendix D.2 for the result of all datasets.

## B.3 Hyperparameter Selection

*MORPH* requires two additional hyperparameters: the history length  $q$  and the maximum regularization weight  $w_{max}$ .

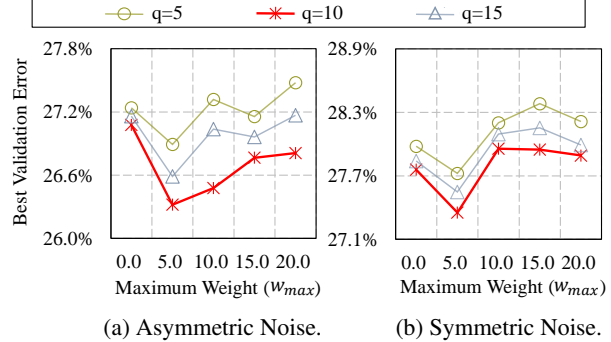


Figure 13: Hyperparameter selection on the CIFAR-100 with two noise types of 40%.

To ascertain the optimal values of these hyperparameters, we trained a WideResNet-16-8 on CIFAR-100 at a noise rate of 40%. Here, because no validation data exists for the CIFAR-100 dataset, we constructed a small clean validation set by randomly selecting 1,000 images from the original training set of 50,000 images. Then the noise injection process was applied to only the rest 49,000 training images. Figure 13 shows the validation errors of *MORPH* obtained by grid search on the noisy CIFAR-100 dataset. The two hyperparameters were chosen in the grid  $q \in \{5, 10, 15\}$  and  $w_{max} \in \{0.0, 5.0, 10.0, 15.0\}$ . Typically, the lowest validation error depending on the history length  $q$  was achieved when the value of  $q$  was 10 for both noise types. As for the maximum weight  $w_{max}$ , the validation error was observed to be the lowest when the value of  $w_{max}$  was 5.0. Therefore, we set the values of  $q$  and  $w_{max}$  to be 10 and 5.0, respectively, in all experiments.

## C Further Details on Experiment Setting

### C.1 Benchmark Datasets

For the experiment, we prepared *five* synthetic or real-world noisy datasets: CIFAR-10<sup>3</sup> (10 classes) (Krizhevsky, Nair, and Hinton 2014) and CIFAR-100<sup>4</sup> (100 classes) (Krizhevsky, Nair, and Hinton 2014), a subset of 80 million categorical images with 50K training images and 10K test images; Tiny-ImageNet<sup>4</sup> (200 classes) (Krizhevsky, Sutskever, and Hinton 2012), a subset of ImageNet with 100K training images and 10K test images; WebVision V1<sup>5</sup> (1000 classes) (Li et al. 2017), real-world noisy data of crawled images using the concepts in ImageNet with 2.4M training images, 50K WebVision validation images, and 50K ImageNet ILSVRC12 validation images; FOOD-101N<sup>6</sup> (101 classes) (Lee et al. 2018), real-world noisy data of crawled food images with 310K training images and 25K FOOD-101 validation images. Following the previous work (Chen et al. 2019), we only used the first 50 classes of the Google image subset in WebVision V1.

Because CIFAR and Tiny-ImageNet are clean, we artificially corrupted the labels in these datasets using typical

<sup>3</sup><https://www.cs.toronto.edu/~kriz/cifar.html>

<sup>4</sup><https://www.kaggle.com/c/tiny-imagenet>

<sup>5</sup><https://data.vision.ee.ethz.ch/cvl/webvision/dataset2017.html>

<sup>6</sup><https://kuanghuei.github.io/Food-101N>

methods for the evaluation of synthetic noises (Han et al. 2018; Yu et al. 2019). For  $k$  classes, we applied the label transition matrix  $\mathbf{T}$ : (i) *symmetric noise*:  $\forall_{j \neq i} \mathbf{T}_{ij} = \frac{\tau}{k-1}$  and (ii) *asymmetric noise*:  $\exists_{j \neq i} \mathbf{T}_{ij} = \tau \wedge \forall_{k \neq i, k \neq j} \mathbf{T}_{ik} = 0$ , where  $\mathbf{T}_{ij}$  is the probability of the true label  $i$  being flipped to the corrupted label  $j$  and  $\tau$  is the noise rate. For the asymmetric noise, the corrupted label  $j$  was set to be the next label of the true label  $i$  following the recent work (Song, Kim, and Lee 2019; Yu et al. 2019).

## C.2 Training Configurations for Real-World Data

To verify the practical usability of *MORPH* on real-world noisy labels, we performed a classification task on WebVision V1 and FOOD-101N. We followed the experimental configurations in the previous work (Chen et al. 2019; Lee et al. 2018; Li et al. 2020). For WebVision V1, we trained an InceptionResNet-V2 from scratch for 120 epochs using SGD with a momentum of 0.9 and an initial learning rate of 0.1, which was divided by 10 after 40 and 80 epochs (refer to (Chen et al. 2019)). For FOOD-101N, we trained a ResNet-50 with the ImageNet pretrained weights for 60 epochs using SGD with a momentum of 0.9 and an initial learning rate of 0.01, which was divided by 10 after 30 epochs (refer to (Lee et al. 2018)). Regardless of the dataset, we used a batch size of 64, a dropout of 0.4, and a weight decay of 0.001. Random crops and horizontal flips were applied for data augmentation.

## C.3 Algorithm Hyperparameters

For reproducibility, we clarify the hyperparameter setup of all compared algorithms. Please note, if the true noise rate  $\tau$  was needed as one of the hyperparameters (in *Co-teaching*, *Co-teaching+*, *ITLM*, and *SELFIE*), then it was set to be the estimated noise rate  $\hat{\tau}$  by *MORPH*, as shown in Figure 9, for fair comparison. The other hyperparameters for each method are configured favorably as follows:

- ***Co-teaching(+)***: To decrease the number of selected samples gradually at the beginning of the training, the warm-up epoch is required as a hyperparameter; it was set to be 15, which is reported to achieve the best performance in the original paper (Han et al. 2018).
- ***INCV***: Following the original paper (Chen et al. 2019), the total number of training rounds was set to be 4; the network was trained for 50 epochs using the Adam optimizer; an initial learning rate was set to be 0.001, which was divided by 2 after 20 and 30 epochs and finally fixed to be 0.0001 after 40 epochs. Subsequently, all the training samples selected by *INCV* were used to retrain the network using *Co-teaching* with the same configuration.
- ***ITLM***: Because it iterates the training process multiple times as well, the total number of training rounds was set to be 5. As mentioned in the original paper (Shen and Sanghavi 2019), the training process for the first 4 rounds was early stopped because it may help filter out false-labeled samples. Subsequently, without early stopping, the network was retrained using the samples selected from the 4th round during the last training round.

Noise Type	Sym. Noise			Asym. Noise	
Noise Rate	20%	40%	70%	20%	40%
DM-DYR-SH	28.0	32.2	46.4	31.1	46.3
DivdeMix	25.3	27.6	<b>38.9</b>	25.4	44.1
<b>MORPH</b>	<b>23.6</b>	<b>27.4</b>	39.5	<b>23.0</b>	<b>26.3</b>

Table 4: Best test errors (%) of *MORPH* compared with DM-DYR-SH and DivdeMix using CIFAR-100.

- ***SELFIE***: Four hyperparameters are required for *SELFIE*. The warm-up epoch for sample selection was set to be 15 similar to *Co-teaching*. The uncertainty threshold and the history length for loss correction were set to be 0.05 and 15, respectively, which are the best values obtained from a grid search in the original paper (Song, Kim, and Lee 2019). The training process was restarted twice according to the authors’ recommendation.

## C.4 Comparison with More Recent Methods

*DM-DYR-SH* (Arazo et al. 2019) and *DivideMix* (Li, Socher, and Hoi 2020) are similar to *MORPH* in that they also use mixture models for handling noisy labels. However, the mixture model is used for a *different* purpose: *DM-DYR-SH* and *DivideMix* use the mixture model to identify clean samples based on the *small-loss* trick; on the other hand, *MORPH* use the model to find the best transition point. In addition, *MORPH* no longer relies on the *small-loss* trick, and incrementally identifies a better set of clean samples through our alternating scheme in Phase II.

Nevertheless, we compared *MORPH* with *DM-DYR-SH* and *DivideMix* for a more in-depth analysis. The results are summarized in Table 4. Only *MORPH* achieved the noise type robustness; the performance of *DM-DYR-SH* and *DivideMix* was considerably worse in asymmetric noise because their underlying philosophy is based on the *small-loss* trick. In fact, *DM-DYR-SH* and *DivideMix* are favored because they are equipped with an unsupervised or semi-supervised method such as *Beta Mixture* (Ma and Leijon 2011) and *MixMatch* (Berthelot et al. 2019) to further improve the performance, while *MORPH* deals with only sample selection. Please note that this superior performance of *MORPH* was achieved even without adopting the unsupervised or semi-supervised method. *MORPH* is expected to perform even much better when combined with such an additional technique.

## D Complete Experiment Results

### D.1 Test Error with Synthetic Noises

Table 5 shows the *test error* of seven training methods using WideResNet-16-8 on three *simulated* noisy datasets with varying noise rates. Two variants of *MORPH* depending on the existence of the consistency regularization were included for comparison

### D.2 Training Time with Synthetic Noises

Table 6 shows the *training time* of seven training methods using WideResNet-16-8 on three *simulated* noisy datasets with varying noise rates.

Noise Type	Asymmetric Noise in Figure 4			Symmetric Noise in Figure 5		
Data Set	CIFAR-10	CIFAR-100	Tiny-Image	CIFAR-10	CIFAR-100	Tiny-Image
<i>Co-teaching</i>	6.92	23.3	41.8	6.77	23.5	40.1
<i>Co-teaching+</i>	9.43	28.9	48.1	10.0	30.9	51.8
<i>INCV</i>	6.16	25.7	44.8	5.82	25.2	44.5
<i>ITLM</i>	6.55	24.6	42.1	6.43	23.3	41.0
<i>SELFIE</i>	6.23	22.4	40.3	5.93	22.3	39.6
<b><i>MORPH</i> w/o. <math>\mathcal{J}(\theta)</math></b>	<b>5.59</b>	<b>22.1</b>	39.6	<b>5.28</b>	<b>21.8</b>	39.2
<b><i>MORPH</i> w. <math>\mathcal{J}(\theta)</math></b>	5.71	22.4	<b>39.3</b>	5.61	22.5	<b>38.7</b>

(a) Best and last test errors under asymmetric and symmetric noises of 10% ( $\tau = 0.1$ ).

Noise Type	Asymmetric Noise in Figure 4			Symmetric Noise in Figure 5		
Data Set	CIFAR-10	CIFAR-100	Tiny-Image	CIFAR-10	CIFAR-100	Tiny-Image
<i>Co-teaching</i>	8.76	26.4	44.6	8.26	24.9	43.4
<i>Co-teaching+</i>	11.6	34.6	54.8	13.7	37.0	58.3
<i>INCV</i>	7.77	28.2	48.1	6.53	26.6	45.7
<i>ITLM</i>	6.58	25.8	45.1	6.69	25.7	43.6
<i>SELFIE</i>	6.59	23.8	42.7	6.74	24.1	41.9
<b><i>MORPH</i> w/o. <math>\mathcal{J}(\theta)</math></b>	<b>5.88</b>	<b>22.8</b>	41.1	<b>5.92</b>	<b>23.2</b>	<b>41.4</b>
<b><i>MORPH</i> w. <math>\mathcal{J}(\theta)</math></b>	5.89	23.0	<b>40.7</b>	6.03	23.6	<b>41.4</b>

(b) Best and last test errors under asymmetric and symmetric noises of 20% ( $\tau = 0.2$ ).

Noise Type	Asymmetric Noise in Figure 4			Symmetric Noise in Figure 5		
Data Set	CIFAR-10	CIFAR-100	Tiny-Image	CIFAR-10	CIFAR-100	Tiny-Image
<i>Co-teaching</i>	13.0	32.3	50.5	10.2	27.5	45.2
<i>Co-teaching+</i>	16.3	42.9	60.9	17.1	45.0	62.7
<i>INCV</i>	12.1	34.9	54.5	7.87	28.2	47.5
<i>ITLM</i>	7.43	29.2	52.5	7.36	27.0	45.8
<i>SELFIE</i>	8.64	27.6	45.0	8.83	26.4	44.4
<b><i>MORPH</i> w/o. <math>\mathcal{J}(\theta)</math></b>	6.11	24.2	43.7	6.85	25.8	43.7
<b><i>MORPH</i> w. <math>\mathcal{J}(\theta)</math></b>	<b>5.97</b>	<b>23.7</b>	<b>43.0</b>	<b>6.83</b>	<b>25.7</b>	<b>43.2</b>

(c) Best and last test errors under asymmetric and symmetric noises of 30% ( $\tau = 0.3$ ).

Noise Type	Asymmetric Noise in Figure 4			Symmetric Noise in Figure 5		
Data Set	CIFAR-10	CIFAR-100	Tiny-Image	CIFAR-10	CIFAR-100	Tiny-Image
<i>Co-teaching</i>	24.7	44.8	61.8	12.4	30.2	48.8
<i>Co-teaching+</i>	21.3	53.3	66.5	20.3	53.7	64.2
<i>INCV</i>	22.2	47.0	63.8	9.43	30.1	49.7
<i>ITLM</i>	12.9	41.9	63.9	8.43	29.3	49.0
<i>SELFIE</i>	13.5	38.6	55.4	10.4	28.2	48.4
<b><i>MORPH</i> w/o. <math>\mathcal{J}(\theta)</math></b>	7.25	27.1	48.9	8.27	27.8	47.0
<b><i>MORPH</i> w. <math>\mathcal{J}(\theta)</math></b>	<b>6.34</b>	<b>26.3</b>	<b>47.2</b>	<b>8.01</b>	<b>27.4</b>	<b>46.2</b>

(d) Best and last test errors under asymmetric and symmetric noises of 40% ( $\tau = 0.4$ ).

Table 5: Best and last test errors (%) of seven training methods on two types of **synthetic** noises with varying noise rates (10%, 20%, 30%, and 40%) in Figures 4 and 5.

Noise Type	Asymmetric Noise in Figure 4			Symmetric Noise in Figure 5		
Data Set	CIFAR-10	CIFAR-100	Tiny-Image	CIFAR-10	CIFAR-100	Tiny-Image
<i>Co-teaching</i>	16,217	15,575	68,404	16,443	15,527	70,409
<i>Co-teaching+</i>	15,051	14,834	80,450	14,834	16,581	80,440
<i>INCV</i>	38,338	33,048	122,771	38,217	32,844	123,247
<i>ITLM</i>	23,341	22,162	79,246	23,701	22,384	83,371
<i>SELFIE</i>	30,894	31,107	121,787	31,319	31,107	123,663
<b><i>MORPH</i> w/o. <math>\mathcal{J}(\theta)</math></b>	<b>9,048</b>	<b>9,358</b>	<b>39,361</b>	<b>9,173</b>	<b>9,361</b>	<b>40,003</b>
<b><i>MORPH</i> w. <math>\mathcal{J}(\theta)</math></b>	12,442	12,091	53,009	12,229	12,182	50,495

(a) Training time under asymmetric and symmetric noises of 10% ( $\tau = 0.1$ ).

Noise Type	Asymmetric Noise in Figure 4			Symmetric Noise in Figure 5		
Data Set	CIFAR-10	CIFAR-100	Tiny-Image	CIFAR-10	CIFAR-100	Tiny-Image
<i>Co-teaching</i>	15,382	14,563	64,710	15,351	14,103	65,121
<i>Co-teaching+</i>	15,019	16,936	82,391	15,229	17,169	82,639
<i>INCV</i>	35,456	30,520	113,722	35,707	30,261	113,208
<i>ITLM</i>	22,192	20,759	74,358	22,102	20,460	74,875
<i>SELFIE</i>	30,992	30,650	119,234	30,916	30,359	66,473
<b><i>MORPH</i> w/o. <math>\mathcal{J}(\theta)</math></b>	<b>9,258</b>	<b>9,497</b>	<b>39,102</b>	<b>9,363</b>	<b>9,412</b>	<b>39,677</b>
<b><i>MORPH</i> w. <math>\mathcal{J}(\theta)</math></b>	12,296	11,840	50,747	12,046	12,259	49,020

(b) Training time under asymmetric and symmetric noises of 20% ( $\tau = 0.2$ ).

Noise Type	Asymmetric Noise in Figure 4			Symmetric Noise in Figure 5		
Data Set	CIFAR-10	CIFAR-100	Tiny-Image	CIFAR-10	CIFAR-100	Tiny-Image
<i>Co-teaching</i>	14,672	13,898	61,922	14,092	12,989	59,299
<i>Co-teaching+</i>	15,285	17,230	83,036	15,390	17,394	83,279
<i>INCV</i>	33,161	28,484	107,899	32,594	27,549	105,857
<i>ITLM</i>	21,018	19,477	70,823	19,972	18,381	66,473
<i>SELFIE</i>	30,728	30,120	118,978	30,619	29,573	117,016
<b><i>MORPH</i> w/o. <math>\mathcal{J}(\theta)</math></b>	<b>9,604</b>	<b>9,491</b>	<b>39,641</b>	<b>9,346</b>	<b>9,484</b>	<b>40,114</b>
<b><i>MORPH</i> w. <math>\mathcal{J}(\theta)</math></b>	11,220	11,775	52,242	11,875	12,175	49,446

(c) Training time under asymmetric and symmetric noises of 30% ( $\tau = 0.3$ ).

Noise Type	Asymmetric Noise in Figure 4			Symmetric Noise in Figure 5		
Data Set	CIFAR-10	CIFAR-100	Tiny-Image	CIFAR-10	CIFAR-100	Tiny-Image
<i>Co-teaching</i>	14,107	13,386	60,262	13,171	11,886	53,660
<i>Co-teaching+</i>	15,527	17,244	82,982	15,365	17,459	80,038
<i>INCV</i>	30,376	26,628	104,597	28,915	24,668	99,314
<i>ITLM</i>	20,068	18,212	69,037	18,763	16,749	60,469
<i>SELFIE</i>	29,730	28,352	115,208	29,436	27,931	113,380
<b><i>MORPH</i> w/o. <math>\mathcal{J}(\theta)</math></b>	<b>9,646</b>	<b>9,477</b>	<b>39,728</b>	<b>9,598</b>	<b>9,488</b>	<b>40,154</b>
<b><i>MORPH</i> w. <math>\mathcal{J}(\theta)</math></b>	11,198	11,828	50,594	11,331	12,049	49,412

(d) Training time under asymmetric and symmetric noises of 40% ( $\tau = 0.4$ ).

Table 6: Training time (sec) of seven training methods on two types of **synthetic** noises with varying noise rates (10%, 20%, 30%, and 40%) in Figures 4 and 5.